A Monte Carlo Simulation Scheme for Nonideal Dendrimers Satisfying Detailed Balance

G. Giupponi* and D. M. A. Buzza

Polymer IRC, Department of Physics & Astronomy, University of Leeds, Leeds LS2 9JT, UK

Received March 13, 2002; Revised Manuscript Received July 2, 2002

ABSTRACT: We present a configurational-biased lattice Monte Carlo scheme for simulating nonideal dendrimers that satisfies detailed balance. This corrects an important shortcoming in a previous lattice Monte Carlo scheme by Mansfield and Klushin: in a previous publication, we showed that the Mansfield and Klushin scheme did not obey detailed balance, and that this led to surprisingly large errors in the radius of gyration R_g and scattering form factor $P(q)$ for ideal dendrimers. In this paper, we have calculated the radius of gyration, the form factor, and the intramolecular density profile for $g = 1-8$ *self-avoiding* dendrimers and find that our results are qualitatively the same as previous results obtained by Mansfield and Klushin (g is the generation number). This indicates that the error in the Mansfield and Klushin scheme due to detailed balance violation is much smaller for self-avoiding dendrimers. Our other key conclusions concerning the equilibrium properties of self-avoiding dendrimers are the following: (1) The radius of gyration scales with the total number of monomers roughly as $R_g \propto N^{1/3}$. A more careful analysis however shows that there is a small (∼30%) and nonmonotonic variation in the internal density of the dendrimer with N, the form and magnitude of which are consistent with previous intrinsic viscosity results on dendrimers. (2) The intramolecular density profile is dense core like at low dendrimer generations ($g < 5$) and solid sphere like at high generations ($g \geq 5$). (3) There is some "hollowness" in the core region of the dendrimer for higher generation dendrimers ($g \geq 5$), though the depth and extent of the hollowness are much smaller than that predicted by the dense shell model. (4) Terminal groups of the dendrimer are not localized at the periphery but delocalized throughout the dendrimer. The relationship between our findings and previous theoretical and experimental studies, especially recent scattering studies on dendrimers, is discussed.

1. Introduction

Dendrimers are highly branched molecules with highly controlled structures and a large number of terminal groups. Their unique molecular topology gives rise to many striking static and dynamic properties and offer potential applications in areas as diverse as drug delivery, chemical catalysis, viscosity modification, etc.[1,2] A key to utilizing and harnessing many of the interesting properties of dendrimers lies in understanding their molecular configurations under different conditions of interest. Because of their exciting properties, the molecular structure of dendrimers has been the subject of intense theoretical[3−11] and experimental[12−18] study over the past 10 years.

The aim of this paper is to study the equilibrium properties of nonideal dendrimers (i.e., where there is nonzero interaction between monomers) using lattice Monte Carlo simulation. A lattice Monte Carlo scheme for simulating dendrimers that is widely referenced in the literature is that of Mansfield and Klushin[5,10] (hereafter referred to as the MK scheme). This scheme has the advantage that it is elegant and samples phase space efficiently. However, in a previous publication[19] we showed that the MK scheme does not obey detailed balance. In the case of ideal (i.e., phantom) dendrimers, this led to suprisingly large errors in the radius of gyration R_g and single particle scattering form factor $P(q)$ compared to known analytical results. In this paper, we propose a lattice configurational-biased Monte Carlo scheme that is applicable to nonideal dendrimers and which obeys detailed balance. Specifically, we shall use a simple cubic lattice and consider dendrimers with a core functionality of three and a spacer length of five lattice steps. This is in contrast to the MK scheme which uses a diamond lattice and a spacer length of seven lattice steps. However, we do not expect these minor differences in microscopic details to lead to any significant differences in the large-scale dendrimer properties.

To check whether the imposition of detailed balance leads to similarly large errors for self-avoiding dendrimers, we have calculated the radius of gyration, radial density profiles, and scattering form factors for self-avoiding dendrimers. In fact, we find that our results are qualitatively the same as previous results obtained from the MK scheme. This indicates that the error in the MK scheme due to the violation of detailed balance is much smaller for self-avoiding dendrimers compared to ideal dendrimers. We discuss the possible reasons for this in the discussion and conclusions section of this paper.

To identify the other issues that will be addressed in this paper, in what follows, we give a brief review of previous theoretical and experimental work on dendrimers. The first major theoretical study of dendrimer properties was performed by deGennes and Hervet using self-consistent-field theory.[3] Assuming that the monomers of each generation lie in successive concentric shells of their own, they predicted a monomer density profile which has a minimum in the center (i.e., the core) of the dendrimer and which grows monotonically to the outer edge (i.e., a dense shell morphology). They also predicted that the radius of the dendrimer scales with the number of monomers as $R \propto N^{1/5}$ below limiting

* Corresponding author: e-mail phygg@irc.leeds.ac.uk.

10.1021/ma0203851 CCC: $22.00
Published on Web 11/01/2002

generation (above the limiting generation, i.e., the generation above which perfect dendritic growth is no longer possible, deGennes and Hervet predict and one expects $R \propto N^{1/3}$ corresponding to a compact space filling object). In contrast, Lescanec and Muthukumar[4] using a kinetic growth algorithm found the terminal spacers to be distributed throughout the molecule with the significant backfolding of dendritic branches leading to a density profile that is maximum in the center and decreases monotonically going away from the center (i.e., a dense core morphology). They found the dendrimer radius to scale with the number of monomers as $R \propto N^{0.5}$ for low N (or generation) and $R \propto N^{0.22\pm0.02}$ for high N. Their high N result therefore agrees with deGennes and Hervet to within simulation error. Using a self-consistent-field method, but relaxing the constraint that monomers of each generation lie in successive concentric shells of their own, Boris and Rubinstein[7] found a radial density profile very similar to Lescanec and Muthukumar, i.e., a dense core morphology with end monomers delocalized throughout the molecule.

Mansfield and Klushin using the MK scheme,[5,10] Murat and Grest[6] and Karatasos et al.[11] using molecular dynamics, Lyulin et al.[8] using Brownian dynamics, and Scherrenberg et al.[14] using molecular dynamics with atomistic detail also find the terminal groups to be delocalized throughout the molecule with the maximum density occurring in the interior rather than the periphery of the dendrimer. However, there are important differences in the density profiles found by these authors compared to the profiles found by Lescanec and Muthukumar and Boris and Rubinstein: (1) Above a system-dependent generation number, the density profile develops a well-developed plateau, the width of which broadens with increasing generation number g. This is akin to the density profile of a solid compact object. At larger distances this uniform density decreases monotonically to zero. (2) Around the same value of g where a density plateau develops, the density profile also develops a small but discernible minimum around the core region[20] (though the extent and depth of this minimum are much smaller than what is predicted by the dense shell model). In terms of the R vs N scaling, in contrast to deGennes and Hervet and Lescanec and Muthukumar, Murat and Grest find $R \propto N^{1/3}$ before the limiting generation is reached. However, Mansfield[10] using the MK scheme finds that the intrinsic viscosity for dendrimers goes through a maximum (in his simulation at $g = 6$). Analyzing Mansfield's results in terms of the scaling relation $R \propto N^{\alpha}$, his results indicate that $\alpha > {}^1/_3$ at low g and $\alpha < {}^1/_3$ at high g. This is in agreement with the predictions of Lescanec and Muthukumar but in conflict with Murat and Grest.

More recently, a number of experimental papers have appeared seeking to elucidate the structure of dendrimers. The R vs molecular weight M scaling for dendrimers has been studied by Prosa et al.[13] via small-angle X-ray scattering (SAXS), by Scherrenberg et al.[14] via small-angle neutron scattering (SANS) and viscometry, and by Evmenenko et al.[18] via SANS, and all these authors find $R \propto M^{1/3}$, in agreement with Murat and Grest[6] but in contrast to deGennes and Hervet,[3] Lescanec and Muthukumar,[4] and Mansfield.[10] However, earlier viscometry results from Mourey et al.[12] show that the intrinsic viscosity for dendrimers goes through a maximum (in their system at around $g = 3$), in agreement with the predictions of Lescanec and Muthukumar[4,12] and Mansfield.[10]

Prosa et al.[13] have also studied the detailed monomer concentration profile of $g = 2-9$ dendrimers (using our counting convention for g) via SAXS and find that for $g = 6-9$ dendrimers the scattering form factors were best fit using a uniform monomer density profile. This is akin to the hard-sphere density profile found by the authors in refs 5, 6, 9, 10, 11, and 14. However, within the accuracy of their data, Prosa et al. were not able to discern a minimum near the core. Potschke et al.[15,17] studying $g = 4$, 5 dendrimers using SANS found by Fourier inversion of their scattering form factor that the monomer density profile exhibits a maximum at the center which decays monotonically going away from the center. This is akin to the dense core density profile found by Lescanec and Muthukumar[4] and Boris and Rubinstein.[7]

To our knowldge, the most direct experimental study probing the position of terminal groups in dendrimers is that of Topp et al.[16] Using SANS with deuterium labeling and scattering contrast matching, Topp et al. found for a $g = 6$ dendrimer (using our counting convention for g) that the radius of gyration of deuterated terminal units was significantly larger than the radius of gyration of the whole dendrimer. They interpreted these data as indicating that dendrimers have terminal groups that are concentrated near the periphery. This is in agreement with the results of deGennes and Hervet but in opposition to virtually all other theoretical studies. We note however that Lyulin, Davies and Adolf,[8,9] using Brownian dynamics simulation, have shown that similar relative differences between the radius of gyration for terminal monomers and the whole dendrimer are obtained from dendrimers where it is known that terminal spacers are delocalized throughout the molecule; their study indicates that great care needs to be taken when inferring the location of terminal groups from a comparison of the radius of gyration for terminal monomers and the whole dendrimer.

In summary, the overwhelming theoretical concensus (apart from the study of deGennes and Hervet) is that dendrimers consisting of flexible spacers do not have a dense shell morphology but instead have a density that is maximum in the interior of the dendrimer with the density tailing off to zero going toward the periphery of the dendrimer. In particular, the self-consistent-field study by Boris and Rubinstein shows conclusively that the dense shell morphology of deGennes and Hervet is an artifact of their assumption that monomers of each generation lie in successive concentric shells of their own, rather than being a consequence of self-consistent theory itself. Experimental studies of the dendrimer density profile[13,15,17] support this general theoretical concensus. However, clearly there are still discrepancies between the different studies (both theoretical and experimental) concerning a number of important issues:

1. What is the correct scaling of R with N?

2. What is the correct dendrimer density profile? Is it dense core like or solid sphere like?

3. Is there any "hollowness" near the core above a critical generation number?

4. Are the terminal groups delocalized throughout the molecule, or are they localized near the periphery of the molecule? Specifically, how do the theoretically pre-

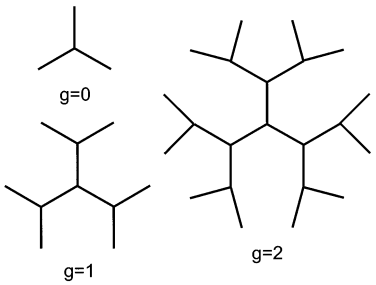

Figure 1. Spacer connectivity for $g = 0$, 1, 2 dendrimers.

dicted relative differences in radius of gyration compare to the values measured by Topp et al.?[16]

The aim of this paper is to address all of these issues via lattice Monte Carlo simulation.The rest of the paper is organized as follows. In section 2 we give details of our configurational-biased Monte Carlo scheme. The results of our simulation and the comparison to previous theoretical results (including the MK scheme) and experimental results are presented in section 3, and section 4 contains our conclusions.

2. Details of Monte Carlo Simulation

We consider a dendrimer laid out on a cubic lattice, and we use units of length where the lattice step length $b = 1$. The central core of the dendrimer is connected to three spacers. Each of these spacers is connected to two other spacers, and they in turn are connected to two other spacers, etc., so that the number of spacers increases by a factor of 2 going from one generation to the next. The connectivity between spacers for the first few generations of dendrimers is illustrated in Figure 1. All spacers in the dendrimer consist of five-step walks on the lattice. The choice of a this short spacer length is motivated by the fact that most dendrimers studied in practice have short spacer lengths. Note that we use the counting convention for the generation number g where a three arm star is considered to be a $g = 0$ dendrimer.

In this paper, we shall be considering self-avoiding dendrimers where no two monomers are allowed to occupy the same lattice site. This corresponds to dendrimers in an athermal solvent where the only relevant interaction between monomers is short-range hard-core repulsions. In practice, it is hard to generate initial dendrimer configurations that are self-avoiding walks; we therefore tolerate monomer overlaps at the initial stages of the simulation but include a large energy penalty U for monomer overlaps; i.e., the energy for placing monomer i at lattice position $\mathbf{r}_i$ is

$$U_i = Ux(\mathbf{r}_i) \tag{1}$$

where $x(\mathbf{r}_i)$ is a counter for the number of monomers already present at lattice position $\mathbf{r}_i$ ($x(\mathbf{r}_i) = 0$ if the lattice site is unoccupied). For $U = 50kT$, which is the value used in our simulations, we find that the number of monomer overlaps rapidly falls to zero in the course of the simulation.

In our simulation, a Monte Carlo move begins with a random selection of a spacer in the dendrimer. Following the MK scheme, we distinguish between two types of trial moves depending on whether the selected spacer belongs to the last generation (i.e., an "end spacer") or to a generation other than the last (i.e., an "internal spacer"). If the chosen spacer is an end spacer, an "end wiggle" is performed, which involves only the end spacer itself. If an internal spacer is chosen, we perform an "internal" wiggle, which involves the selected internal spacer and its two daughters. Together these form a three-legged "spider" (see Figure 2).

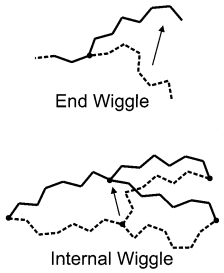

Figure 2. End wiggle and internal wiggle.

In the MK scheme, the end wiggle is performed by replacing the configuration of the chosen spacer by another spacer configuration which is chosen with equal probability from all possible spacer configurations. An internal wiggle on the other hand is performed by keeping the three "feet" of the spider (i.e., the nodes where the legs of the spider terminate) stationary, while displacing the central node of the spider to one of the next-nearest-neighbor positions, which is chosen with equal probability from all the possible next-nearest-neighbor positions. Spacer states having the correct end-to-end vector are then chosen at random in order to bridge the gaps between each foot of the spider and the new central node position. In ref 19, we showed that this procedure for performing internal wiggle trial moves together with the acceptance probability used in the MK scheme violated detailed balance.

In contrast to the MK scheme (which is a Metropolis Monte Carlo scheme), we perform end wiggles and internal wiggles using a configurational-bias Monte Carlo (CBMC) scheme.[22] The main feature of CBMC is that trial moves are no longer chosen at random but are biased in such a way as to enhance the acceptance probability of the new configuration. To satisfy detailed balance (and hence remove the bias that was introduced in generating trial configurations), one is required to modify the acceptance probability from that of Metropolis Monte Carlo (see below). Although CBMC tends to be more complicated compared to Metropolis Monte Carlo, for some systems, CBMC can speed up the calculation considerably. In the context of dendrimer simulations, CBMC has at least two advantages. First, CBMC provides a very natural way for us to perform internal wiggles which satisfy detailed balance (see subsection 2.2). Second, we can bias our trial moves energetically so that the trial states generated have minimal monomer overlaps. This becomes a distinct advantage when simulating dendrimers of high generation where the intramolecular monomer concentrations are high and where the acceptance probability for standard Metropolis trial moves can become very low because of the high probability of monomer overlaps. In what follows, we describe how we perform end wiggles and internal wiggles and give other simulation details.

2.1. End Wiggle. Once we have removed the old terminal spacer configuration o, we build the new terminal spacer trial configuration n monomer by monomer. In a cubic lattice, there are six possible trial directions for each monomer. We choose the jth trial

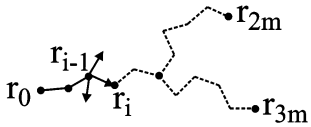

Figure 3. Generating an internal wiggle trial move in the CBMC scheme.

direction for the ith monomer with probability

$$P_i(j) = \frac{\exp[-\beta U_i(j)]}{w_i} \tag{2}$$

where $\beta \equiv 1/kT$, $U_i(j)$ is the energy of placing the ith monomer in the jth trial direction given by eq 1, and

$$w_i = \sum_{j'=1}^{6} \exp[-\beta U_i(j')] \tag{3}$$

The probability for making the trial move $o \rightarrow n$ is therefore given by

$$\alpha(o \rightarrow n) = \prod_{i=1}^{m} P_i(n) = \frac{\exp[-\beta U(n)]}{W(n)} \tag{4}$$

where m (=5) is the total number of monomers in the spacer, $U(n) = \sum_{i=1}^{m} U_i(n)$ is the total energy of the trial configuration n, and

$$W(n) = \prod_{i=1}^{m} w_i(n) \tag{5}$$

is the Rosenbluth factor of n. We next remove the trial configuration and retrace the old configuration o and calculate its Rosenbluth factor $W(o)$ in the process using eqs 3 and 5. Finally, to satisfy detailed balance, the trial move $o \rightarrow n$ is accepted with probability[22]

$$acc(o \rightarrow n) = \min\left(1, \frac{W(n)}{W(o)}\right) \tag{6}$$

Note that the acceptance probability eq 6 is different from the one used in Metropolis Monte Carlo.

2.2. Internal Wiggle. We first remove all the monomers belonging to the chosen internal spacer and its two daughters (which together have configuration o) and rebuild the trial configuration n. One complication in constructing the trial configuration n is the fact that three-legged spiders with one leg connected to $\mathbf{r}_0$ are required to have the other two legs terminating at $\mathbf{r}_{2m}$ and $\mathbf{r}_{3m}$ (see Figure 3). We can achieve this by including the following additional bias in the construction of trial configurations. For the parent spacer ($i = 1 \rightarrow 5$), the probability for placing monomer i in the jth trial step is

$$P_i(j) = \frac{\exp[-\beta U_i(j)]\Omega_3(\mathbf{r}_{i-1} + \Delta\mathbf{r}_j, \mathbf{r}_{2m}, \mathbf{r}_{3m};\, m - i)}{\sum_{j'=1}^{6} \exp[-\beta U_i(j')]\Omega_3(\mathbf{r}_{i-1} + \Delta\mathbf{r}_{j'}, \mathbf{r}_{2m}, \mathbf{r}_{3m};\, m - i)}$$

$$= \frac{\exp[-\beta U_i(j)]}{w_i} \frac{\Omega_3(\mathbf{r}_{i-1} + \Delta\mathbf{r}_j, \mathbf{r}_{2m}, \mathbf{r}_{3m};\, m - i)}{\sum_{j'=1}^{6} \Omega_3(\mathbf{r}_{i-1} + \Delta\mathbf{r}_{j'}, \mathbf{r}_{2m}, \mathbf{r}_{3m};\, m - i)} \tag{7}$$

where $\Omega_3(\mathbf{r}_{i-1} + \Delta\mathbf{r}_j, \mathbf{r}_{2m}, \mathbf{r}_{3m}; m - i)$ is the number of ideal (i.e., phantom) three-legged spider configurations that start at the trial position of the ith monomer $\mathbf{r}_{i-1} + \Delta\mathbf{r}_j$ and terminate at $\mathbf{r}_{2m}$ and $\mathbf{r}_{3m}$, the length of the spacers connected to $\mathbf{r}_{i-1} + \Delta\mathbf{r}_j$, $\mathbf{r}_{2m}$, and $\mathbf{r}_{3m}$ being $m - i$, m, and m, respectively (see Figure 3). The function Ω_3 can be calculated beforehand and stored as a (6-dimensional) array (see Appendix A). The normalization factor w_i is given by

$$w_i = \frac{\sum_{j=1}^{6} \exp[-\beta U_i(j)]\Omega_3(\mathbf{r}_{i-1} + \Delta\mathbf{r}_j, \mathbf{r}_{2m}, \mathbf{r}_{3m};\, m - i)}{\sum_{j=1}^{6} \Omega_3(\mathbf{r}_{i-1} + \Delta\mathbf{r}_j, \mathbf{r}_{2m}, \mathbf{r}_{3m};\, m - i)} \tag{8}$$

Once we have finished constructing the trial configuration for the parent spacer, we proceed to construct the two daughter spacers in turn (the choice of which daughter to construct first is made randomly). For the daughter spacers ($i = 6 \rightarrow 10$ and $i = 11 \rightarrow 15$), the probability for placing monomer i in the jth trial step is given by eqs 7 and 8 but with Ω_3 replaced by $\Omega_2(\mathbf{r}_{i-1} + \Delta\mathbf{r}_j, \mathbf{r}_{km}; m - i)$, i.e., the number of ideal linear chain configurations with length $m - i$ starting at $\mathbf{r}_{i-1} + \Delta\mathbf{r}_j$ and ending at $\mathbf{r}_{km}$ ($\mathbf{r}_{km} = \mathbf{r}_{2m}$ and $\mathbf{r}_{3m}$ respectively for the first and second daughter). Ω_2 can be calculated analytically and is given in Appendix A.

The probability of making the trial move $o \rightarrow n$ is now given by

$$\alpha(o \rightarrow n) = \prod_{i=1}^{3m} P_i(n) = \frac{\exp[-\beta U(n)]}{W(n)\ \Omega_3(\mathbf{r}_0, \mathbf{r}_{2m}, \mathbf{r}_{3m}; m)} \tag{9}$$

where $U(n) = \sum_{i=1}^{3m} U_i(n)$ is the total energy of the trial configuration n and

$$W(n) = \prod_{i=1}^{3N} w_i(n) \tag{10}$$

is the Rosenbluth factor of n. The final equality in eq 9 can be obtained by noting that $\Omega_3(\mathbf{r}_{i-1}, \mathbf{r}_{2m}, \mathbf{r}_{3m}; m - i + 1) = \sum_{j=1}^{6} \Omega_3(\mathbf{r}_{i-1} + \Delta\mathbf{r}_j, \mathbf{r}_{2m}, \mathbf{r}_{3m}; m - i)$. We note that the factor $\Omega_3(\mathbf{r}_0, \mathbf{r}_{2m}, \mathbf{r}_{3m}; m)$ in eq 9 is the same for both $o \rightarrow n$ and $n \rightarrow o$. The procedure outlined above guarantees that only trial configurations consisting of three-legged spiders starting at $\mathbf{r}_0$ and terminating at $\mathbf{r}_{2m}$ and $\mathbf{r}_{3m}$ are generated. For high enough overlap energies U, the procedures in this and the previous subsection also generate trial configurations which have minimal overlap with other monomers.

We next remove the trial configuration and retrace the old configuration o and calculate its Rosenbluth factor $W(o)$ in the process using eqs 8 and 10. Finally, to satisfy detailed balance, the trial move $o \rightarrow n$ is accepted with probability[22]

$$acc(o \rightarrow n) = \min\left(1, \frac{W(n)}{W(o)}\right) \tag{11}$$

2.3. Other Simulation Details. Two different techniques were used to generate initial configurations for the Monte Carlo simulations. In the first technique, which produces what we call "random" initial structures, the initial state of all the spacers in the dendrimer are

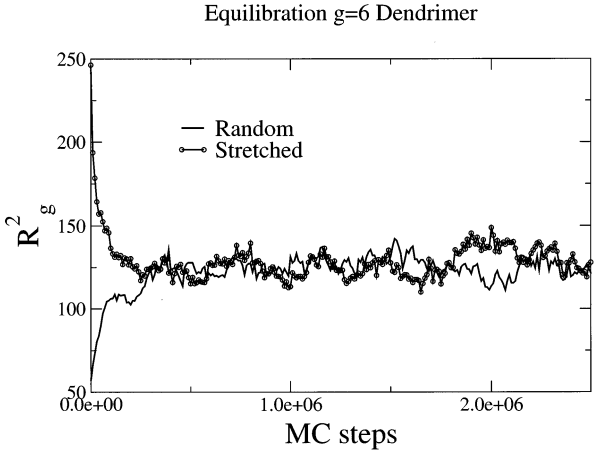

Figure 4. Relaxation of the radius of gyration for a $g = 6$ self-avoiding dendrimer starting from stretched and random initial structures. N_{eq} is determined as the point where the two runs first converge to the same average value.

Table 1. Number of Monte Carlo Steps Required for Equlibration (N_{eq}), the Autocorrlation Interval (τ), and the Total Number of MC Steps xN_{eq} Used in Our Simulations for Each Dendrimer Generation

g	N_{eq}	τ	x
1	10^4		500
2	10^4		500
3	10^4		500
4	10^4	7.5×10^3	500
5	5×10^4	2.5×10^4	500
6	2.5×10^5	10^5	250
7	10^6		100
8	6×10^6		50

[a]The quoted values of N_{eq} for $g = 1-3$ are in fact larger than necessary.

generated by randomly selecting trial directions for each monomer. In the second technique, which produces what we call "stretched" initial structures, a strong radial force is applied to all the monomers in a random initial structure until a highly stretched structure is produced. This artificial radial force is then switched off and the resultant dendrimer configuration used as the initital structure for the Monte Carlo simulation. We note that both these methods generate initial structures that contain monomer overlaps. However, by imposing a large energy penalty for monomer overlaps, $U = 50kT$, we found that the number of monomer overlaps rapidly falls to zero so that there are no monomer overlaps by the time equilibration is reached. To determine the number of Monte Carlo steps required for equlibration N_{eq} for our simulation, we performed two parallel runs for each generation of dendrimer, starting from the two different initial structures outlined above. We define the point where the radius of gyration (R_g) from the two runs first converge to the same average value as the point where thermal equilibrium has been achieved. For example, in Figure 4 we show the radius of gyration results for a $g = 6$ dendrimer. According to our criterion, thermal equilibrium had been achieved at $N_{eq} = 2.5 \times 10^5$ Monte Carlo steps. The values for N_{eq} are reported in Table 1 for each dendrimer generation. (The quoted values of N_{eq} for $g = 1-3$ are in fact larger than necessary.)

To ensure good statistics for averaging, runs of xN_{eq} Monte Carlo steps were performed for each simulation, where the value of x for each dendrimer generation is reported in Table 1 ($x = 50-500$). At intervals of N_{eq} steps, the configuration of the dendrimer was sampled for the following properties: (1) The radius of gyration squared for the whole molecule and terminal spacers only, R_g^2 and R_{ge}^2, respectively. (2) The radial density of all monomers ρ_i and terminal monomers only ρ_{ei}, where ρ_i and ρ_{ei} are the number of monomers and terminal monomers, respectively, over the number of lattice sites in the ith shell, where the ith shell is the region of space whose radial distance r from the core is $i - 1 < r \leq i$ (the $i = 1$ shell includes monomers at the central core as well). (3) The scattering form factor for the whole molecule and terminal spacers only, $P(q)$ and $P_e(q)$, respectively. The quantities R_g^2 and $P(q)$ were calculated from

$$R_g^2 = \frac{1}{2N^2}\sum_{j=1}^{N}\sum_{k=1}^{N}(\mathbf{r}_j - \mathbf{r}_k)^2 \tag{12}$$

$$P(q) = \frac{1}{N^2}\sum_{j=1}^{N}\sum_{k=1}^{N}\frac{\sin(q|\mathbf{r}_j - \mathbf{r}_k|)}{q|\mathbf{r}_j - \mathbf{r}_k|} \tag{13}$$

where $\mathbf{r}_j$ is the position vector of the jth monomer, q is the magnitude of the scattering wave vector, and $N = 3m(2^{g+1} - 1) + 1$ is the total number of monomers in the dendrimer (including the central core), where $m = 5$ is the number of monomers in a spacer. The quantities R_{ge}^2 and $P_e(q)$ were calculated from eqs 12 and 13 but with the double sums summing over terminal monomers only, and N was replaced by the total number of terminal monomers $N_e = 3m \times 2^g$. Because data points are collected at intervals of N_{eq} steps, the data points are essentially independent of each other so that we can quantify the errors in our simulation easily; e.g., the error in R_g^2 is $\sigma/\sqrt{x}$, where σ is the variance of R_g^2 calculated from our simulation.

An alternative and perhaps more accurate measure of the sampling interval that is required before the samples can be considered to be independent is the autocorrelation interval τ (in terms of number of MC steps). This can be defined via the normalized autocorrelation function of the squared radius of gyration

$$C_{R_g}(t) = \frac{\langle R_g^2(t_0)\, R_g^2(t_0 + t)\rangle - \langle R_g^2\rangle^2}{\langle R_g^4\rangle - \langle R_g^2\rangle^2} \tag{14}$$

where $R_g^2(t_0)$ and $R_g^2(t_0 + t)$ are the squared radius of gyration after t_0 and $t_0 + t$ MC steps, respectively, and the angled brackets indicate averages over the simulation after thermal equilibrium has been achieved. (The first angled bracket in the numerator in eq 14 is averaged over t_0.) We define τ as the interval where $C_{R_g}(\tau) = e^{-1}$, and τ values for $g = 4, 5, 6$ are reported in Table 1. In Figure 5, we show the autocorrelation function for a $g = 6$ dendrimer, where according to our definition $\tau \approx 10^5$. We note that in all cases τ is roughly a factor of 2 less than N_{eq}. This indicates that using a sampling interval of N_{eq} is adequate to obtain data points which are essentially independent.

In our previous paper,[19] we presented analytical results for R_g^2 and $P(q)$ for ideal dendrimers. As a benchmark, we have checked our CBMC simulation results for R_g^2 and $P(q)$ in the ideal dendrimer limit (i.e., $U = 0$) against these analytical results. We used the same total number of Monte Carlo steps and sampling frequency as the corresponding self-avoiding dendrimer

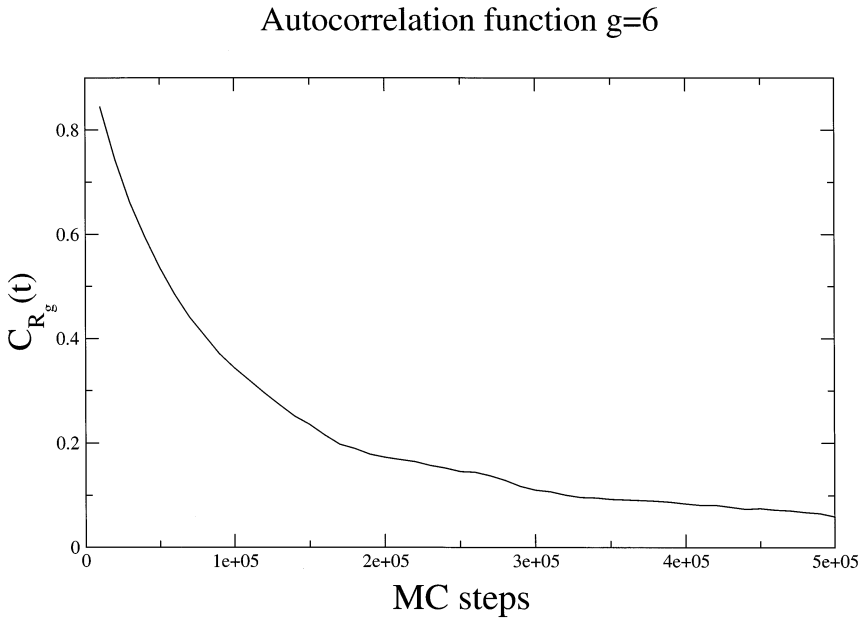

Figure 5. Normalized autocorrelation function of the squared radius of gyration for a $g = 6$ self-avoiding dendrimer.

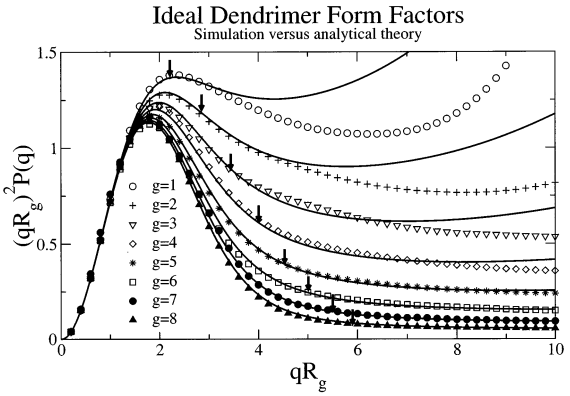

Figure 6. Kratky plot of scattering form factor for $g = 1-8$ ideal dendrimers comparing our CBMC simulation (data points) with the exact analytical calculation (solid lines).

for these benchmark simulations. The simulation and analytical results for R_g for $g = 1-8$ ideal dendrimers are collected in Table 1. We find excellent agreement (within simulation errors) between simulation and analytical theory. The fact that our estimated simulation error correctly reflects the typical discrepancy between simulation and the exact results confirms that our sampling interval is adequate to ensure that the data points are essentially independent. In Figure 6, we present Kratky plots of $(qR_g)^2P(q)$ vs (qR_g) comparing our simulation to the exact analytical results for $g = 1-8$ ideal dendrimers. Again, we find excellent agreement between simulation and analytical theory. Discrepancies at high q and low g in Figure 6 are due to differences in the microscopic details of the two approaches: the exact calculation assumed an off-lattice Gaussian chain model for the polymer chains while the simulation was performed for polymers on a lattice. We expect the agreement between the two approaches to breakdown for $qb \gtrsim 1$. In Figure 6, the point where $qb = 1$ for each g is indicated by an arrow. We see that in fact the agreement between simulation and analytical theory extends considerably beyond $qb = 1$. These benchmark simulations give us confidence that our simulation code is correct and obeys detailed balance. They also show that the total length of the MC runs and sampling frequency used in this study are sufficient to obtain accurate simulation data for the dendrimer quantities of interest.

3. Results and Discussion

3.1. Scaling of R_g vs N. In Table 2, we report results (including error bars) for the radius of gyration of the whole dendrimer R_g and for terminal monomers only R_g for $g = 1-8$ self-avoiding dendrimers. In Figure 7, we present a log−log plot of R_g vs N. We find the data to roughly obey the scaling $R_g \propto N^{0.33\pm0.01}$, suggesting that the dendrimer behaves like a compact, space-filling object with constant density (i.e., fractal dimension of 3) over the range of g values studied. This is in agreement with the molecular dynamics study of Murat and Grest[6] and numerous experimental studies mentioned in the Introduction.[13,14,18] However, examining the data in Figure 7 more carefully, we discern a small but systematic deviation of the data from the constant density scaling $R_g \propto N^{1/3}$. This deviation is made more apparent in Figure 8 where we present a plot of the inverse density R_g^3/N vs N. Here we clearly see that the density of the dendrimer varies nonmonotonically with N (or g), and the inverse density goes through a maximum at around $g = 3$ in our simulation. Assuming that the intrinsic viscosity $[\eta]$ scales roughly as R_g^3/N, our data are in good agreement with the nonmonotonic variation of the intrinsic viscosity $[\eta]$ found experimentally by Mourey et al.[12] and theoretically by Lescanec and Muthukumar[4,21] and Mansfield[10] using the MK scheme. In particular, the magnitude of the inverse density variation in our simulation agrees with the intrinsic viscosity variation found in these studies to within a factor of 2. For example, the ratio of the maximum inverse density to the inverse density at $g = 1$ is 1.3 in our simulation, while the ratio of the maximum intrinsic viscosity to the intrinsic viscosity at $g = 1$ is 1.3 in the viscometry study of Mourey et al. and 2.4 in the Monte Carlo simulation of Mansfield.[10] (The agreement between our results and Mansfield can be made more quantitative by recognizing that the ratio of the hydrodynamic radius R_h to R_g is not constant but

Table 2. Simulation Results for Ideal Dendrimers and Self-Avoiding Dendrimers

	ideal dendrimers		self-avoiding dendrimers			
g	R_g (theory)	R_g (simulation)	R_g	R_{ge}	Δ	R_g^3/N
1	2.21	2.19 ± 0.02	3.12 ± 0.02	3.53 ± 0.02	0.129 ± 0.008	0.662 ± 0.009
2	2.85	2.88 ± 0.02	4.36 ± 0.02	5.01 ± 0.02	0.148 ± 0.006	0.781 ± 0.009
3	3.45	3.44 ± 0.02	5.75 ± 0.02	6.55 ± 0.02	0.140 ± 0.005	0.839 ± 0.006
4	4.01	4.02 ± 0.02	7.23 ± 0.02	8.05 ± 0.02	0.113 ± 0.004	0.812 ± 0.006
5	4.53	4.53 ± 0.02	9.08 ± 0.02	9.90 ± 0.02	0.090 ± 0.003	0.792 ± 0.004
6	5.02	5.07 ± 0.03	11.24 ± 0.02	12.06 ± 0.02	0.073 ± 0.002	0.745 ± 0.004
7	5.47	5.41 ± 0.05	13.80 ± 0.03	14.62 ± 0.03	0.059 ± 0.003	0.687 ± 0.004
8	5.90	5.89 ± 0.06	16.96 ± 0.03	17.70 ± 0.03	0.044 ± 0.003	0.636 ± 0.003

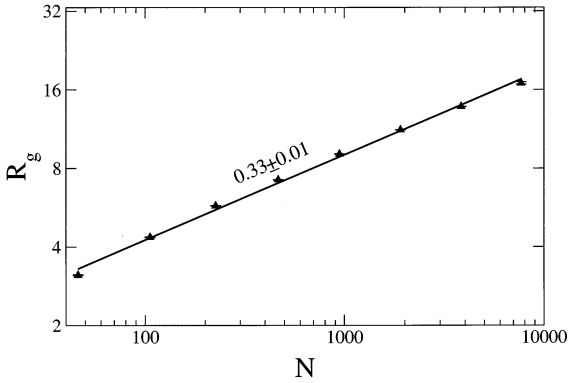

Figure 7. Plot of log−log of R_g vs N together with best fit line $R_g \propto N^{0.33\pm0.01}$ for self-avoiding dendrimers. The error bars are smaller than the symbol size.

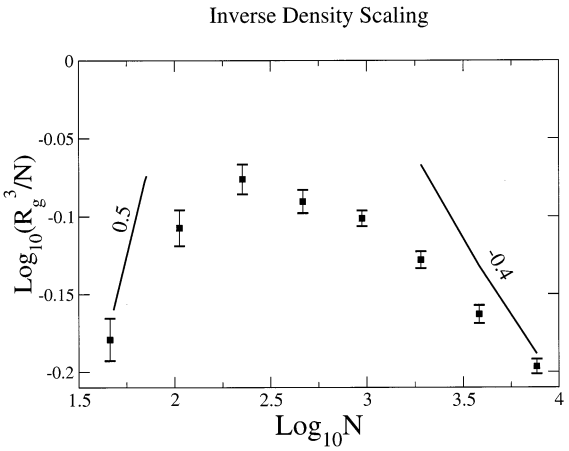

Figure 8. Plot of log R_g^3/N vs log N together with the low and high N scaling predictions of Lescanec and Muthukumar for self-avoiding dendrimers.

varies with g by about 50%.[10]) Our analysis shows that it is possible to reconcile the $R_g \propto N^{1/3}$ scaling observed by Murat and Grest,[6] Prosa et al.,[13] Scherrenberg et al.,[14] and Evmenenko et al.[18] with the nonmonotonic variation of $[\eta]$ with N found by Lescanec and Muthukumar,[4,21] Mourey et al.,[12] and Mansfield[10] because the variation in the density with molecular weight is small (only ∼30% in our simulation). In terms of R_g vs N, a ∼30% variation in density is equivalent to a ∼10% variation in R_g from the constant density scaling of $R_g \propto N^{1/3}$; this would be very hard to detect on a log−log plot. Plotting R_g^3/N vs N therefore represents a more sensitive way to pick out any subtle variations away from constant density scaling compared to plotting R_g vs N.

This nonmonotonic variation of dendrimer density with generation was first predicted by Lescanec and Muthukumar;[4] they predicted that $R_g^3/N \propto N^{0.5}$ at low N and $R_g^3/N \propto N^{-0.4}$ at high N. We include these scaling predictions in Figure 8. Clearly, our data do not follow their predicted scaling at high and low N. We believe that this is due to the nonequilibrium nature of the kinetic growth algorithm used by Lescanec and Muthukumar. Their scaling predictions therefore pertain to the specific nonequilibrium ensemble of structures generated by their algorithm and not to the well-equilibrated dendrimer structures used in our study.

3.2. Radial Density Profiles. In Figure 9a,b, we plot the radial density profile for all monomers ρ_i and terminal monomers only ρ_{ei} for $g = 3-8$ dendrimers, where ρ_i and ρ_{ei} are the number of monomers and terminal monomers, respectively, over the number of lattice sites in the ith shell, where the ith shell is the region of space whose radial distance r from the core is $i - 1 < r \leq i$ (the $i = 1$ shell includes monomers at the central core as well). In what follows we shall use r and i interchangeably, since they are roughly the same, especially at large i. For all the dendrimers, a core region of very high density is apparent near the center; this high density rapidly decreases within two lattice spacings from the core. For $g = 1-4$ dendrimers, this rapid decrease is followed by a more gradual monotonic decrease of the density to zero, which is akin to the dense core morphology found by Lescanec and Muthukumar and Boris and Rubinstein. (The data for $g = 1$, 2 dendrimers are not shown in Figure 9 but follow this trend.) However for $g \geq 5$, the rapid density decrease is followed by a local minimum at around $r = 3$, which in turn is followed by a density plateau. The width of this constant density region increases with increasing generation so that for $g = 8$ it extends to about $r = 16$. Finally at even higher r, the density plateau tails off to zero.

We note that our radial density profiles are in good qualitatively agreement with results obtained from the MK scheme.[5,10] This indicates that the error in the MK scheme due to detailed balance violation is small for the radial density profiles of self-avoiding walk dendrimers. Our density profiles for $g \geq 5$ are also in good agreement with the molecular dynamics simulations of Murat and Grest[6] and Karatasos, Adolf, and Davies[11] and are akin to a solid sphere morphology, albeit with a small local minimum near the core; the extent and depth of this minimum are much smaller though compared to the dense shell morphology predicted by deGennes and Hervet.[3] Our results for $g \geq 5$ are however inconsistent with the results of Lescanec and Muthukumar[4] and Boris and Rubinstein,[7] who find a dense core profile (with no minimum near the core) even for higher generation dendrimers. The difference bewteen our radial density profiles and the dense core profile is especially striking when one looks at scattering form factors, as we shall see in subsection 3.4.

Boris and Rubinstein have correctly pointed out that the local minimum in the density profile occurs in the

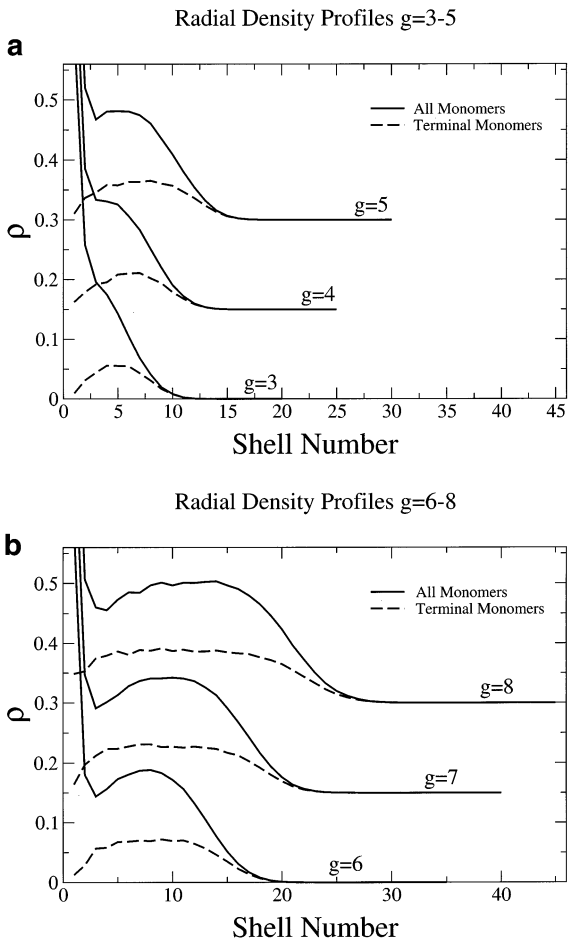

Figure 9. Radial density profile of monomers (solid lines) and terminal monomers (dashed lines) for (a) $g = 3-5$ and (b) $g = 6-8$ self-avoiding dendrimers; the curves for $g = 4$, 7 are shifted vertically by 0.15, and the curves for $g = 5$, 8 are shifted vertically by 0.3 for clarity.

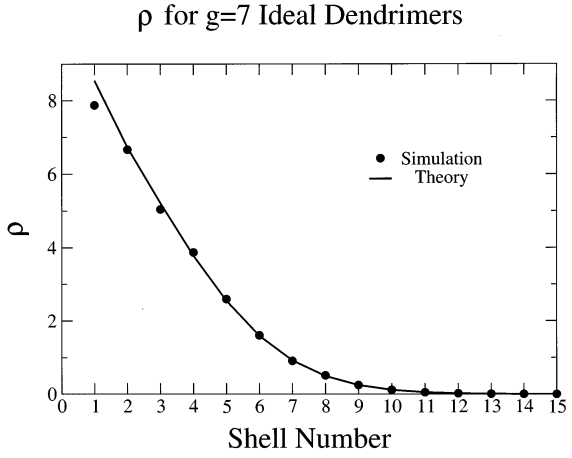

Figure 10. Radial density profile of monomers for a $g = 7$ ideal dendrimer; simulation (data points) vs analytical theory (solid line).

region where the simulation data (including ours) is least reliable due to poor statistics. To determine whether this local minimum exists, it is therefore imperative that one quantifies the simulation error in this small r region. In Figure 10 we compare our simulation results for ρ_i for a $g = 7$ ideal dendrimer (i.e., $U = 0$) with the exact analytical result for ρ_i which is derived explicitly in Appendix B. The simulation data in Figure 10 are obtained from MC runs of $100N_{eq}$ steps sampling every N_{eq} steps, i.e., using the same protocol as for a $g = 7$ self-avoiding dendrimer. We find excellent agreement between simulation and the exact results for $r \geq 2$, indicating that our simulation results are accurate for $r \geq 2$. We expect the accuracy of our simulation data in the small r region to be even greater for self-avoiding dendrimers compared to ideal dendrimers because the presence of excluded-volume interactions should strongly suppress concentration fluctuations. Since the local minima in Figure 9a,b occur in the region where $r \geq 2$, we conclude that they are real features of the density profile for dendrimers with $g \geq 5$.

We believe that the difference between the solid sphere like density profile (with the small density minimum near the core) predicted by us and other authors[5,6,10,11,14] and the dense core profile found by Lescanec and Muthukumar is due to the nonequilibrium nature of the Lescanec−Muthukumar model, as explained in the previous subsection. On the other hand, the dendrimer structures in the self-consistent-field study of Boris and Rubinstein are well-annealed, so the differences in the radial density profiles found by us and Boris and Rubinstein clearly arise from a different source. We believe the difference in this case may be due to the considerably smaller effective excluded-volume parameter used by Boris and Rubinstein (see Figures 6 and 8 in ref 7). The high effective excluded-volume used in our study and in refs 5, 6, 9−11, and 14 causes the monomer density to saturate (at intermediate values of r) while the much softer monomer interaction potentials used by Boris and Rubinstein means that no such saturation is seen. We may also qualitatively understand the local minimum observed in our study and in refs 5, 6, 9−11, and 14 as being due to an attempt by the dendrimer to lower its overall free energy: by stretching the central spacers, the dendrimer is able increase its overall volume (thereby relieving the high excluded-volume interaction energy) by paying only a small entropic penalty (a few kT) corresponding to stretching the few central spacers. The lack of a minimum in the study of Boris and Rubinstein could be due to the considerably lower excluded volume parameter removing the driving force for such a minimum.

Experimentally, Prosa et al.[13] have studied the detailed monomer concentration profile of $g = 2-9$ dendrimers (using our counting convention for g) via SAXS and found that for $g = 6-9$ dendrimers the scattering form factors contained higher order peaks (up to three higher order peaks for $g = 9$). This result cannot be explained by the dense core density profile which does not produce any higher order peaks (see subsection 3.4). Instead, Prosa et al. find that their scattering form factors for $g = 6-9$ dendrimers were best fit using a solid sphere density profile, consistent with our study and those in refs 5, 6, 9−11, and 14. This suggests that real dendrimers with short spacer lengths tend to have a large effective excluded-volume parameter. Potschke et al.[15,17] studying $g = 4$, 5 dendrimers using SANS found by Fourier inversion of their scattering form factor that the monomer density profile resembles the dense core profile predicted by Lescanec and Muthukumar[4] and Boris and Rubinstein.[7] This is also consistent with our study as we find that low generation dendrimers ($g \leq 4$ in our simulation) exhibit a dense core like density profile. However, we note that in their study the scattering wavevector only goes up to $qR_g = 4-5$. It

would be helpful to go up to marginally higher qR_g values (≈6) in order to definitely rule out the presence of higher order peaks in the form factor, thereby confirming that the density profile is dense core like rather than solid sphere like.

In the studies of Prosa et al.[13] and Potschke et al.,[15,17] no evidence for any "hollowness" near the core was found. For the SANS study of Potschke et al., this absence may be due to the relatively low g values of their dendrimers; we recall that in our simulation a minimum was only exhibited for dendrimers with $g \geq 5$. However, given that the length scale of the minimum is considerably smaller compared to the overall size of the dendrimer (see Figure 9a,b), it would again be helpful to go to higher qR_g to definitively rule out such a feature in their dendrimers. For the SAXS study of Prosa et al., their scattering wavevector goes up to $qR_g \approx 15$ for their $g = 9$ dendrimer (using our counting convention for g). We estimate that this should be high enough to discern a minimum near the core. Despite this, no hollowness was detected by Prosa et al. We mention two points that may be relevant to this issue. First, a recent paper by Mansfield[10] using the MK scheme has shown that for very high generation dendrimers ($g = 11$ in his simulation) the minimum disappears. Assuming that the imposition of detailed balance does not qualitatively change this result, this could explain why no minimum was discerned by Prosa et al. for $g = 9$ dendrimers. Second, we note that one of the density profiles used by Prosa et al. to fit their form factors contain a density minimum in the center (i.e., the "sphere with hole" profile; see Figure 9 in ref 13). This profile gave reasonable though not the best fits. It is possible therefore that the presence of a small minimum near the center may still be consistent with their scattering data. It would be interesting to perform a direct inversion of the form factor (which is possible since the density profile is centrosymmetric) to see whether any evidence for a density minimum at the center can be found.

3.3. Location of Terminal Groups. In Figure 9a,b, we have plotted the radial density profiles for terminal monomers together with the density profile of all monomers. Clearly, for all dendrimer generations investigated in this study, the terminal groups are distributed throughout the molecule. This is in agreement with virtually all previous theoretical studies. However, using SANS with deuterium labeling and scattering contrast matching, Topp et al.[16] found that for a $g = 6$ PAMAM dendrimer (using our counting convention for g) the radius of gyration of deuterated terminal units, $R_{ge} = 39.3 \pm 1.0$ Å, was significantly greater than the radius of gyration of the whole dendrimer, $R_g = 34.4 \pm 0.2$ Å. They interpreted their data as indicating that the terminal groups are concentrated near the periphery of the dendrimer. In terms of the relative difference[8,9]

$$\Delta = \frac{R_{ge} - R_g}{R_g} \tag{15}$$

their results give $\Delta = 0.14 \pm 0.03$. However, Lyulin, Davies, and Adolf[8,9] have pointed out that the fact $R_{ge} > R_g$ (i.e., $\Delta > 0$) does not necessarily imply that the terminal groups are localized at the periphery. To illustrate this, they studied the terminal group distribution for a $g = 5$ dendrimer using Brownian dynamics: they found that the Δ value for this system ($\Delta = 0.10 \pm 0.03$) was close to the value found by Topp et al. (the error bars overlap); however, it is clear that the terminal spacers in their simulation are in fact delocalized throughout the molecule. The study of Lyulin, Davies, and Adolf demonstrates the important point that one cannot infer that the terminal groups are localized at the periphery solely from the fact that $R_{ge} > R_g$ (i.e., $\Delta > 0$). Instead, in terms of the relative difference Δ, one requires the experimental value of Δ to be significantly greater than simulation values before significant localization of terminal groups near the periphery can be inferred.

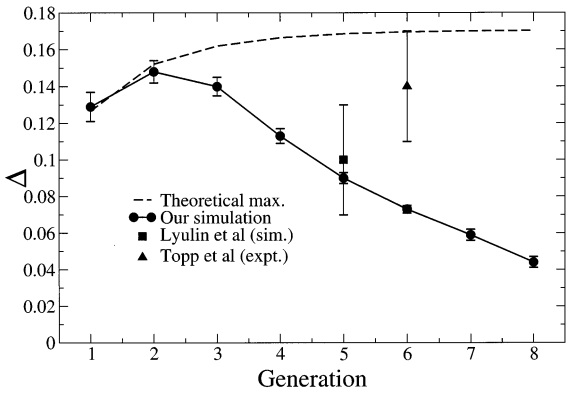

Figure 11. Our simulation results for Δ vs g for self-avoiding dendrimers. Simulation results of Lyulin et al. for $g = 5$, experimental results of Topp et al. for $g = 6$ (using our counting convention for g), and the theoretical upper bound for Δ (dashed curve) are also shown.

Mansfield[10] has calculated R_g and R_{ge} using the MK scheme for $g = 1-9$. For $g = 6$, Mansfield's results give $\Delta = 0.074$, which is significantly smaller than the value $\Delta = 0.14 \pm 0.03$ found by Topp et al. However, the violation of detailed balance by the MK scheme introduces uncertainties into Mansfield's results. In Table 2, we present our simulation results for R_g, R_{ge}, and Δ for $g = 1-8$ self-avoiding dendrimers. Interestingly, our value for Δ for $g = 6$ ($\Delta = 0.073 \pm 0.002$) agrees with the value obtained from the MK scheme. This indicates that the error in calculating R_g and R_{ge} in the MK scheme due to the violation of detailed balance is probably much smaller for self-avoiding dendrimers compared to ideal dendrimers.

Our results for Δ as a function of g are plotted in Figure 11 together with the experimental Δ values of Topp et al. and the theoretical Δ values of Lyulin et al. We note first of all that there is a significant variation of Δ with g in our simulation. We also note that for $g = 5$ our value for Δ ($= 0.090 \pm 0.003$) agrees with Lyulin et al.'s value ($\Delta = 0.10 \pm 0.03$) to within simulation errors. This indicates that, in contrast to R_g and R_{ge}, the value of Δ may be rather insensitive to microscopic details (e.g., spacer length, specific simulation technique, etc.) and may be primarily a function of g only. If this is indeed the case, then our simulation curve for Δ in Figure 11 may have some degree of universality, applying to all dendrimers with flexible spacers, in the absence of long-range interactions (e.g., electrostatic interactions). To put both simulation and experimental results into context, we have also estimated the theoretical maximum for Δ as a function of g from the following argument. Consider a dendrimer that has a solid sphere radial density profile and that all the terminal monomers are strongly localized in a spherical shell at the periphery of the dendrimer. We can estimate

the inner and outer radius of the shell from $4\pi r_i^3/3 = N - N_e$ and $4\pi r_0^3/3 = N$, respectively, where N and N_e are the number of all monomers and terminal monomers, respectively (working in units where the monomer length is unity). We can then easily calculate the radius of gyration for the sphere (R_g) and the shell (R_{ge}) from r_0 and r_i.[23] In Figure 11, we have plotted the theoretical maximum value for Δ estimated in this way as a function of g for a spacer length $m = 5$ (dashed line). In fact, we find the value of the theoretical maximum to be rather insensitive to variations in m so that the upper bound for Δ in Figure 11 may again have some degree of universality. From Figure 11, we see that the value of Δ found by Topp et al. for $g = 6$ ($\Delta = 0.14 \pm 0.03$) falls between our simulation value ($\Delta = 0.073 \pm 0.002$) and the theoretical maximum ($\Delta = 0.17$), though it is closer to the latter than the former. This indicates that the terminal groups in the dendrimers measured by Topp et al. are considerably more concentrated near the periphery compared to our predicted terminal group distribution for $g = 6$ in Figure 9b, though they are not perfectly localized at the periphery. We emphasize however that we have arrived at this conclusion from a detailed comparison of Topp et al.'s data with theoretical results, rather than from the fact that $\Delta > 0$.

To be sure, measuring R_g and R_{ge} does not represent a very accurate method for determining the distribution of terminal groups. This is because the values of R_g and R_{ge} can never be very different from each other because the major contribution to R_g comes from terminal monomers (since terminal monomers constitute half of all monomers and they tend to be farther away from the center of mass). In seeking to determine the distribution of terminal groups from the difference of two similar numbers, we inevitably encounter large relative errors in the measurement. This is reflected in the rather small values for Δ relative to the experimental uncertainty, even in the case of the theoretical maximum for Δ. We suggest two alternatives for determining terminal group distribution which should be more accurate. The first is to measure the radius of gyration for internal, i.e., *nonterminal*, spacers R_{gi} and calculate the relative difference $\Delta' = (R_{ge} - R_{gi})/R_{gi}$. This should be possible using SANS with contrast matching. For the idealized scenario mentioned above, we estimate a theoretical maximum of $\Delta' = 0.48$, which is considerably larger than the theoretical maximum for Δ. The second is to perform a direct analysis of the scattering form factor for labeled terminal groups $P_e(q)$. We elaborate on this in the next subsection. It would be interesting to use one of these alternative methods to obtain a more accurate measure of the degree to which the terminal groups in Topp et al.'s dendrimers are localized at the periphery.

3.4. Scattering Form Factors. In Figure 12, we present a Kratky plot of $(qR_g)^2P(q)$ vs qR_g for $g = 1-8$ dendrimers from our simulation data, where R_g and $P(q)$ is the radius of gyration and single particle scattering form factor, respectively, of the entire dendrimer. In Figure 12 we have also plotted $P(q)$ for a particle having a hard sphere profile and a dense core profile for comparison. For the hard sphere profile

$$P_{HS}(q) = \frac{9\pi}{2}\left[\frac{J_{3/2}(X)}{X^{3/2}}\right]^2 \tag{16}$$

where $X = (5/3)^{1/2}qR_g$, $J_{3/2}(x) = (2/\pi x^3)^{1/2}(\sin x - x \cos x)$, and $R_g^2 = (3/5)r^2$, where r is the radius of the sphere.[23] For the dense core profile, we note from the work of Lescanec and Muthukumar[4] and Boris and Rubinstein[7] that the radial density profiles in their simulations resemble a Gaussian profile for dendrimers with $g \geq 6$ (using our counting convention for g). We therefore approximate the form factor for the dense core profile as

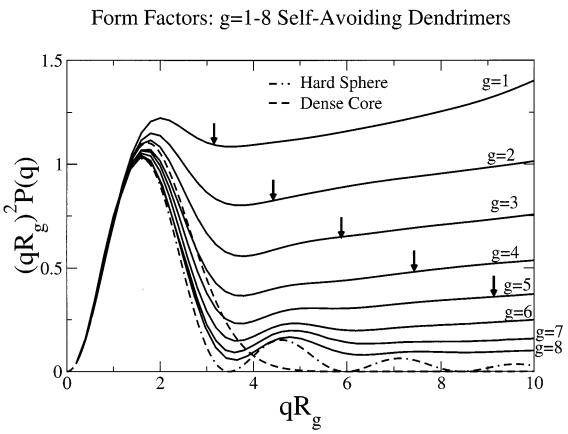

Figure 12. Kratky plot of the scattering form factor $P(q)$ for $g = 1-8$ self-avoiding dendrimers (solid lines), together with the form factor for a hard sphere profile (dot−dashed line) and dense core profile (dashed line). The points where $qb = 1$ for each generation are indicated by arrows.

$$P_{DC}(q) = \exp\left(-\frac{1}{3}q^2R_g^2\right) \tag{17}$$

which is the Guinier form factor.[24] Note that our dense core form factor neglects contributions to the scattering from intradendrimer concentration fluctuations,[7] so that it represents a lower bound for the scattering form factor for $g \geq 6$ dendrimers obeying the Lescanec−Muthukumar model or the Boris−Rubinstein model. (The contribution to the scattering from internal concentration fluctuations is negligible for a hard sphere profile while they are automatically included in our simulation.)

We note from Figure 12 that as we go to higher g, the scattering form factors resemble the hard sphere form factor more and more. In particular, higher order peaks corresponding to solid sphere scattering begin to develop for $g \geq 5$; this is in good agreement with our radial density profile results where we observed a hard sphere like profile beginning to develop for $g \geq 5$. Our results for $P(q)$ agree qualitatively with previous results obtained from the MK scheme.[10] This indicates that the error in the MK scheme due to detailed balance violation is much smaller for the form factor of self-avoiding dendrimers compared to ideal dendrimers. Our results are also in good agreement with the SAXS results of Prosa et al.[13] In contrast, our simulation results for $g \geq 6$ clearly deviate from the dense core form factor for $qR_g > 1$. Most strikingly, our simulation data show higher order scattering peaks while these peaks are completely absent for the dense core model; this is because there is no sharp boundary in the dense core radial density profile to give rise to these higher order peaks.

In Figure 13, we present the Kratky plot of $(qR_{ge})^2P_e(q)$ vs qR_{ge} for a $g = 6$ dendrimer, where R_{ge} and $P_e(q)$ are the radius of gyration and single particle scattering form factor, respectively, for terminal monomers only of the dendrimer. (The choice of g is motivated by the scat-

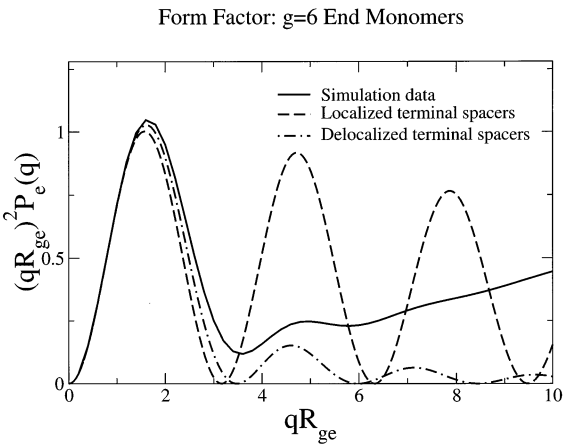

Figure 13. Kratky plot of scattering form factor for terminal monomers $P_e(q)$ for a $g = 6$ self-avoiding dendrimer (solid line). Also plotted are $P_e(q)$ for idealized models where the terminal groups are delocalized (dot−dashed line) and strongly localized at the periphery (dashed line); see text for details.

tering experiments of Topp et al.[16]) In Figure 13 we have also plotted $P_e(q)$ for two idealized models. The first is where the terminal groups are uniformly distributed throughout the dendrimer; this is approximated by using for $P_e(q)$ the hard sphere form factor given earlier. The second is where the terminal groups are strongly localized at the periphery of the dendrimer; this is approximated by using for $P_e(q)$ the form factor for the spherical shell described at the end of the previous subsection. The inner and outer radius of the shell is given by $4\pi r_i^3/3 = N - N_e$ and $4\pi r_0^3/3 = N$, respectively, where N and N_e are the number of all monomers and terminal monomers, respectively, and we consider the case where $g = 6$ and the spacer length $m = 5$. The (normalized) form factor for a spherical shell is given by[23]

$$P_{SH}(q) = \frac{9\pi}{2(1-\alpha^3)^2}\left[\frac{J_{3/2}(X_0)}{X_0^{3/2}} - \alpha^3\frac{J_{3/2}(X_i)}{X_i^{3/2}}\right]^2 \quad (18)$$

where $\alpha = r_i/r_0$, $X_0 = \{(5/3)[(1-\alpha^3)/(1-\alpha^5)]\}^{1/2}qR_g$ and $X_i = \{(5/3)[(1-\alpha^3)/(1-\alpha^5)]\}^{1/2}\alpha qR_g$. From Figure 13, we see that our scattering form factor results for $g = 6$ are much closer to the model where the terminal groups are delocalized compared the model where the terminal groups are strongly localized at the periphery. This is in good agreement with our radial density profile results for terminal groups (Figure 9b) where we see that for $g = 6$ the terminal groups are delocalized throughout the dendrimer. We note that there is large difference between the localized and delocalized models in the amplitude of the second-order peak of the form factor. This was first pointed out by Boris and Rubinstein.[7] We therefore suggest that studying the form factor of terminal monomers $P_e(q)$ up to the second-order scattering peak ($qR_g \approx 6$) provides a much more direct and accurate means for determining the distribution of terminal groups compared to measuring R_g and R_{ge} only.

4. Discussion and Conclusions

In this paper, we have presented a configurational-biased Monte Carlo scheme that obeys detailed balance and is applicable to nonideal dendrimers. We have calculated the radius of gyration, radial density profiles, and scattering form factors for self-avoiding dendrimers and found that our results are qualitatively very similar to previous results obtained using the MK scheme. This indicates that the error in the MK scheme due to the violation of detailed balance is much smaller for self-avoiding dendrimers compared to ideal dendrimers. The reason for this is probably the fact that self-avoiding dendrimers sample a much more restricted subspace of phase space compared to ideal dendrimers. Given that the detailed balance condition dictates the exploration of phase space, it is reasonable to expect that the error due to detailed balance violation will not show up as clearly for self-avoiding dendrimers compared to ideal dendrimers.

From studying $g = 1-8$ dendrimers, our other key conclusions concerning the equilibrium properties of self-avoiding dendrimers are as follows:

1. The radius of gyration scales with the total number of monomers roughly as $R_g \propto N^{1/3}$, suggesting that dendrimers behave like compact space-filling objects. This is in agreement with Murat and Grest[6] and many recent scattering studies on dendrimers.[13,14,18] However, a more careful analysis shows that there is actually a small (∼30%), nonmonotonic variation of the dendrimer internal density with molecular weight or generation, the form and magnitude of which are consistent with previous intrinsic viscosity studies on dendrimers.[4,10,12,21] Our analysis therefore shows that it is possible to reconcile two apparently conflicting views in the literature concerning the scaling of R_g with N because the variation of the internal density is small. It also shows that plotting R_g^3/N vs N provides a more sensitive way to pick out subtle variations away from constant density scaling compared to plotting R_g vs N.

2. The radial density profile is dense core like for low-generation dendrimers ($g < 5$) and hard sphere like for high-generation dendrimers ($g \geq 5$). This is in good agreement with recent scattering studies on dendrimers.[13,15,17]

3. There is some hollowness in the core region of the dendrimer for higher generation dendrimers ($g \geq 5$), though depth and extent of the hollowness are much smaller than that predicted by the dense shell model of deGennes and Hervet.[3]

4. In our model, the terminal groups of the dendrimer are not localized at the periphery but delocalized throughout the dendrimer. Our calculated value of $\Delta = (R_{ge} - R_g)/R_g = 0.07 \pm 0.02$ for a $g = 6$ dendrimer is significantly smaller compared to the value $\Delta = 0.014 \pm 0.03$ found by Topp et al.[16] from SANS measurements of a $g = 6$ dendrimer. This indicates that the terminal groups of Topp et al. are more localized at the periphery compared to our model predictions. We note however that comparing R_g and R_{ge} represents a rather inaccurate method for determining the distribution of end groups, because the values of R_g and R_{ge} can never be very different from each other. We suggest two alternatives which should be more accurate. The first is to compare R_{ge} with R_{gi}, the radius of gyration for *non-terminal* spacers. The second, which follows a suggestion by Boris and Rubinstein,[7] is to study the form factor of terminal monomers up to the second-order scattering peak.

During the preparation of this paper, we became aware of an alternative and complementary Monte Carlo scheme (based on Metropolis Monte Carlo) proposed by Mansfield and Jeong that corrects the MK scheme for detailed balance violation.[25] Mansfield and

Jeong perform a direct quantitative comparison of their new scheme (which obeys detailed balance) with the MK scheme for self-avoiding dendrimers. They find that for self-avoiding dendrimers the errors in the MK scheme are much smaller compared to those for ideal dendrimers, so that previous results from the MK scheme remain qualitatively and even semiquantitatively correct. Our finding on this issue therefore coincides with those of Mansfield and Jeong. Mansfield and Jeong have also calculated Δ as a function of g, and our results agree quantitatively with theirs (within simulation errors). Given that their simulations are performed on a diamond lattice for dendrimers with spacer lengths of seven lattice steps, this further confirms that the Δ vs g curve is rather insensitive to the microscopic details of the simulation, at least for dendrimers with flexible spacers in the absence of long-range interactions.

Acknowledgment. The authors gratefully acknowledge helpful discussions with Dave Adolf, Geoff Davies, and Peter Olmsted. We also thank Prof. Marc Mansfield for giving us access to their manuscript (ref 25) prior to publication. Part of this work has been computed on the Leeds University HPC Modelling Facility partially funded under the 1997 Joint Research Equipment Initiative of the Research and Funding Councils.

Appendix A. Calculation of Ω_3

The function $\Omega_3(\mathbf{r}_1,\mathbf{r}_2,\mathbf{r}_3;n)$ counts the number of ideal three-arm star configurations with arbitrary branch point position but where the end points of the three arms with arm lengths n, m, and m are connected to $\mathbf{r}_1$, $\mathbf{r}_2$, and $\mathbf{r}_3$, respectively ($m = 5$ in our simulation); see Figure 3. Because of translational symmetry, we can set $\mathbf{r}_1 = 0$ without loss of generality so that $\Omega_3 = \Omega_3(\mathbf{r}_2,\mathbf{r}_3;n)$ is in fact a six-dimensional array. Referring to Figure 3, Ω_3 can be expressed as

$$\Omega_3(\mathbf{r}_2,\mathbf{r}_3;n) = \sum_{\mathbf{r}_4} \Omega_2(\mathbf{r}_4;n)\cdot\Omega_2(\mathbf{r}_2 - \mathbf{r}_4;m)\cdot\Omega_2(\mathbf{r}_3 - \mathbf{r}_4;m) \tag{19}$$

where $\Omega_2(\mathbf{r};n)$ counts the number of configurations of a linear chain of length n with end-to-end vector $\mathbf{r}$, $\mathbf{r}_4$ is the branch point position, and we are summing over all possible $\mathbf{r}_4$. The problem of calculating Ω_3 now reduces to the calculation of $\Omega_2(\mathbf{r};n)$. The function $\Omega_2(\mathbf{r};n) \equiv \Omega_2(r_x,r_y,r_z;n)$ can be calculated numerically or analytically. For a cubic lattice, $\Omega_2(\mathbf{r};n)$ has been calculated analytically by other authors.[26] The result is

$$\Omega_2(r_x,r_y,r_z;n) = \sum_{\bar{x}=0}^{n^- - \bar{y}} \sum_{\bar{y}=0}^{n^-} \frac{n!}{\bar{x}!(\bar{x}+|r_x|)!\bar{y}!(\bar{y}+|r_y|)!(n^- - \bar{x} - \bar{y})!(n^+ - \bar{x} - \bar{y})!} \tag{20}$$

for $|r_x| + |r_y| + |r_z| \le n$ *and* Modulo$(r_x + r_y + r_z, 2) =$ Modulo$(n, 2)$, else $\Omega_2(r_x, r_y, r_z;n) = 0$.[27] In eq 20, $n^- = (n - |r_x| - |r_y| - |r_z|)/2$ and $n^+ = (n - |r_x| - |r_y| + |r_z|)/2$. The value of Ω_3 is therefore completely defined by eqs 19 and 20.

In principle, the value for each component of $\mathbf{r}_2$ and $\mathbf{r}_3$ can lie between $-(n + m) \rightarrow +(n + m)$. The function Ω_3 therefore a 6-dimensional array of size $(2n + 2m + 1)^6$, which is very large even for modest values of m and n. However, the size of Ω_3 can be reduced significantly by exploiting its symmetries. In a cubic lattice, these are that $\Omega_3(\mathbf{r}_2,\mathbf{r}_3;n)$ is invariant under the following:

1. changing signs of the components of $\mathbf{r}_2$ *and* $\mathbf{r}_3$, i.e.,

$$\Omega_3(r_{2x}, r_{2y}, r_{2z};r_{3x}, r_{3y}, r_{3z}) = \Omega_3(-r_{2x}, r_{2y}, r_{2z}; -r_{3x}, r_{3y}, r_{3z}) \text{ etc.}$$

2. permutations of components of $\mathbf{r}_2$ *and* $\mathbf{r}_3$, i.e.,

$$\Omega_3(r_{2x}, r_{2y}, r_{2z};r_{3x}, r_{3y}, r_{3z}) = \Omega_3(r_{2y}, r_{2x}, r_{2z};r_{3y}, r_{3x}, r_{3z}) \text{ etc.}$$

Using operations 1 and 2, therefore, we can map an arbitrary $\mathbf{r}_2$ to the region of space where $r_{2x}, r_{2y}, r_{2z} > 0$ and $r_{2x} > r_{2y} > r_{2z}$ without loss of generality. Note that the same operations have to be applied to $\mathbf{r}_3$ as well, but in general, $\mathbf{r}_3$ will be in an arbitrary region of coordinate space. We can therefore represent Ω_3 by an array of size roughly $(n + m) \times (m + n)/2 \times (m + n)/3 \times (2n + 2m + 1)^3$. This represents a reduction in size by a factor of roughly $8 \times 6 = 48$. Within this restricted domain of $\mathbf{r}_2$ and $\mathbf{r}_3$ values, many of the elements of Ω_3 will in fact be zero because of the physical constraints imposed on $\mathbf{r}_2 \equiv (r_{2x}, r_{2y}, r_{2z})$ and $\mathbf{r}_3 \equiv (r_{3x}, r_{3y}, r_{3z})$ by chain connectivity. Specifically, a necessary (but not sufficient) condition that 0, $\mathbf{r}_2$, and $\mathbf{r}_3$ are connected by a three-arm star with arm lengths n, m, and m is that the components of $\mathbf{r}_2$ and $\mathbf{r}_3$ to obey *all* of the conditions below

$$|r_{2x}| + |r_{2y}| + |r_{2x}| \le n + m \tag{21a}$$

$$|r_{3x}| + |r_{3y}| + |r_{3z}| \le n + m \tag{21b}$$

$$|r_{3x} - r_{2x}| + |r_{3y} - r_{2y}| + |r_{3z} - r_{2z}| \le 2n \tag{21c}$$

$$\text{Modulo}(r_{2x} + r_{2y} + r_{2z}, 2) = \text{Modulo}(n + m, 2) \tag{21d}$$

$$\text{Modulo}(r_{3x} + r_{3y} + r_{3z}, 2) = \text{Modulo}(n + m, 2) \tag{21e}$$

$$\text{Modulo}(r_{3x} + r_{3y} + r_{3z} - r_{2x} - r_{2y} - r_{2z}, 2) = \text{Modulo}(2n, 2) = 0 \tag{21f}$$

otherwise $\Omega_3 = 0$.

In our simulation, the function Ω_3 is calculated beforehand within the restricted domain $0 \le r_{2x} \le n + m$, $0 \le r_{2y} \le (n + m)/2$, $0 \le r_{2z} \le (n + m)/3$, $-(n + m) \le r_{3x} \le n + m$, $-(n + m) \le r_{3y} \le n + m$, $-(n + m) \le r_{3z} \le n + m$. Within this domain, $\mathbf{r}_2$ and $\mathbf{r}_3$ are first tested to see whether they satisfy the conditions given by eqs 21a−21f. If they satisfy these conditions, Ω_3 is calculated using eqs 19 and 20; otherwise $\Omega_3 = 0$. These results for Ω_3 are stored as a (6-dimensional) array. When calling the function $\Omega_3(\mathbf{r}_2,\mathbf{r}_3;n)$ in our program, we first test whether $\mathbf{r}_2$ and $\mathbf{r}_3$ satisfy the conditions given by eqs 21a−21f. If they fail the test, $\Omega_3 = 0$. If they pass the test, we perform some simple symmetry operations on $\mathbf{r}_2$ and $\mathbf{r}_3$ so that $\mathbf{r}_2$ lies in the domain of Ω_3 and call Ω_3.

Appendix B. Analytical Calculation of ρ_i for an Ideal Dendrimer

In this appendix, we calculate ρ_i, the monomer density in the ith shell. The starting point of our calculation is the expression for the dendrimer monomer density $\rho(\mathbf{r})$

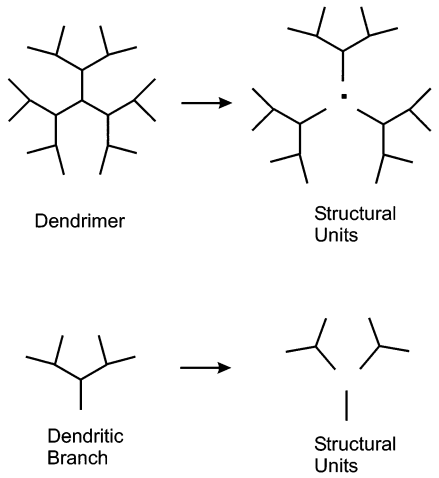

Figure 14. Structural units used to calculate the co-term of a $g = 2$ dendrimer and dendritic branch.

at vector distance $\mathbf{r}$ from the core, which is at position $\mathbf{r}_0$, i.e.,

$$\rho(\mathbf{r}) = \sum_i \delta(\mathbf{r} - (\mathbf{r}_i - \mathbf{r}_0)) \tag{22}$$

where $\mathbf{r}_i$ is the position of the ith monomer and $\delta(\mathbf{r})$ is the delta function. Now the average monomer density at a radial distance r from the core is

$$\bar{\rho}(r) = \langle \rho(\mathbf{r}) \rangle \tag{23}$$

where $\langle \cdots \rangle$ represents an ensemble average over monomer positions. Note that after taking the ensemble average, $\bar{\rho}(r)$ becomes centrosymmetric in r; i.e., it is a function r only. Now the Fourier transform of $\bar{\rho}(r)$ is given by

$$\bar{\rho}(q) = \int \mathrm{d}\mathbf{r}\, \langle \rho(\mathbf{r}) \rangle \exp(i\mathbf{q}\cdot\mathbf{r}) = \sum_i \langle \exp(i\mathbf{q}\cdot(\mathbf{r}_i - \mathbf{r}_0)) \rangle \tag{24}$$

where we have used eqs 22 and 23 to obtain the final equality in eq 24. Given that $\mathbf{r}_0$ is a point on the dendrimer (the core), in the formalism developed by Read for calculating polymer form factors,[28] $\sum_{i\in\gamma} \langle \exp(i\mathbf{q}\cdot(\mathbf{r}_i - \mathbf{r}_0)) \rangle$ is the "co-term" for all the monomers belonging to the structural unit γ, where we are free to define our structural units according to what is most convenient. For the dendrimer, we choose our structural units to be dendritic branches of generation g (see Figure 14). Denoting H_g as the co-term of a generation g dendritic branch, $\bar{\rho}(q)$ for the whole dendrimer is given by

$$\bar{\rho}(q) = n_b H_g + 1 \tag{25}$$

where n_b is the number of dendritic branches connected to the core monomer ($n_b = 3$ in our case) and 1 accounts for the co-term of the core. As we showed in ref 19, H_g can be expressed in terms of the co-terms of dendritic branches of lower generation (see Figure 14), i.e.,

$$H_g = H_0 + 2G_0 H_{g-1} \tag{26}$$

where H_{g-1} is the co-term of a dendritic branch of generation $g - 1$ and H_0 and G_0 are respectively the co-term and "propagator" of a spacer (i.e., a generation 0 dendritic branch). Provided we know H_0 and G_0, therefore $\bar{\rho}(q)$ for the whole dendrimer can be built up iteratively to arbitrary g using eqs 25 and 26. Calculating $\bar{\rho}(q)$ for an ideal dendrimer therefore reduces to the problem of calculating H_0 and G_0.

For a spacer of m monomers, the quantities H_0 and G_0 are given by

$$G_0 = \langle \exp[i\mathbf{q}\cdot(\mathbf{r}_m - \mathbf{r}_0)] \rangle$$

$$H_0 = \sum_{j=1}^{m} \langle \exp[i\mathbf{q}\cdot(\mathbf{r}_j - \mathbf{r}_0)] \rangle$$

where $\mathbf{r}_0$ in the above formulas refer to the position of the monomer to which the spacer is connected adjacent to monomer 1. Assuming a Gaussian chain model for the spacer, the above quantities can be easily calculated, and the result is

$$G_0 = \exp[-mQ_0^2]$$

$$H_0 = \sum_{j=1}^{m} \exp[-jQ_0^2] = \frac{1 - \exp[-mQ_0^2]}{\exp[Q_0^2] - 1}$$

where $Q_0^2 \equiv q^2b^2/6$. Once $\bar{\rho}(q)$ has been calculated, $\bar{\rho}(r)$ can be obtained by performing an inverse Fourier transform. One small complication is the fact that the core contribution to $\bar{\rho}(q)$ causes the inverse Fourier transform to be ill-defined numerically. We therefore remove the core contribution when doing the inverse Fourier transform and add it back in later. The average monomer density excluding the core monomer is given by

$$\bar{\rho}'(r) = \frac{1}{(2\pi)^3}\int \mathrm{d}\mathbf{q}\; n_b H_g(q) \exp(-i\mathbf{q}\cdot\mathbf{r}) = \frac{n_b}{2\pi^2}\int_0^\infty \mathrm{d}q\; H_g(q) q^2 \frac{\sin(qr)}{qr}$$

where the second equality follows from the fact that $H_g(q)$ is centrosymmetric in q. The function $H_g(q)$ decays exponentially in q so that the integral after the second equality is well-defined and can easily be calculated numerically. Finally, the monomer density in the first shell (adding back in the core monomer) is

$$\rho_1 = \frac{3}{4\pi}[1 + \int_0^1 \bar{\rho}'(r) 4\pi r^2\, \mathrm{d}r]$$

while the monomer density in subsequent shells is

$$\rho_i = \frac{3}{4\pi[i^3 - (i-1)^3]}\int_{i-1}^{i} \rho'(r) 4\pi r^2\, \mathrm{d}r \quad \text{for } i = 2, 3, \ldots$$

References and Notes

(1) Voit, B. I. *Acta Polym.* **1995**, *46*, 87−99.
(2) Bosman, A. W.; Janssen, H. M.; Meijer, E. W. *Chem. Rev.* **1999**, *99*, 1665−1688.
(3) Degennes, P. G.; Hervet, H. *J. Phys., Lett.* **1983**, *44*, L351−L360.
(4) Lescanec, R. L.; Muthukumar, M. *Macromolecules* **1990**, *23*, 2280−2288.
(5) Mansfield, M. L.; Klushin, L. I. *Macromolecules* **1993**, *26*, 4262−4268.
(6) Murat, M.; Grest, G. S. *Macromolecules* **1996**, *29*, 1278−1285.
(7) Boris, D.; Rubinstein, M. *Macromolecules* **1996**, *29*, 7251−7260.
(8) Lyulin, A.; Davies, G.; Adolf, D. *Macromolecules* **2000**, *33*, 3294−3304.

(9) Lyulin, A. V.; Davies, G. R.; Adolf, D. B. *Macromolecules* **2000**, *33*, 6899−6900.
(10) Mansfield, M. L. *Macromolecules* **2000**, *33*, 8043−8049.
(11) Karatasos, K.; Adolf, D. B.; Davies, G. R. *J. Chem. Phys.* **2001**, *115*, 5310−5318.
(12) Mourey, T.; Turner, S.; Rubinstein, M.; Frechet, J.; Hawker, C.; Wooley, K. *Macromolecules* **1992**, *25*, 2401−2406.
(13) Prosa, T. J.; Bauer, B. J.; Amis, E. J.; Tomalia, D. A.; Scherrenberg, R. *J. Polym. Sci., Part B: Polym. Phys.* **1997**, *35*, 2913−2924.
(14) Scherrenberg, R.; Coussens, B.; van Vliet, P.; Edouard, G.; Brackman, J.; de Brabander, E.; Mortensen, K. *Macromolecules* **1998**, *31*, 456−461.
(15) Potschke, D.; Ballauff, M.; Lindner, P.; Fischer, M.; Vogtle, F. *Macromolecules* **1999**, *32*, 4079−4087.
(16) Topp, A.; Bauer, B. J.; Klimash, J. W.; Spindler, R.; Tomalia, D. A.; Amis, E. J. *Macromolecules* **1999**, *32*, 7226−7231.
(17) Potschke, D.; Ballauff, M.; Lindner, P.; Fischer, M.; Vogtle, F. *Macromol. Chem. Phys.* **2000**, *201*, 330−339.
(18) Evmenenko, G.; Bauer, B. J.; Kleppinger, R.; Forier, B.; Dehaen, W.; Amis, E. J.; Mischenko, N.; Reynaers, H. *Macromol. Chem. Phys.* **2001**, *202*, 891−899.
(19) Wallace, E.; Buzza, D.; Read, D. *Macromolecules* **2001**, *34*, 7140−7146.
(20) Karatasos et al. find liquidlke correlation peaks superposed on top of what appears to be a local minimum at short distances. The presence of these peaks is probably due to the very short spacers used in their study.
(21) Mansfield, M.; Klushin, L. *J. Phys. Chem.* **1992**, *96*, 3994−3998.
(22) Frenkel, D.; Smit, B. *Understanding Molecular Simulation;* Academic Press: San Diego, 1996.
(23) Burchard, W. *Adv. Polym. Sci.* **1983**, *48*, 1−124.
(24) Burchard, W.; Kajiwara, K.; Nerger, D. *J. Polym. Sci., Phys. Ed.* **1982**, *20*, 157−171.
(25) Mansfield, M. L.; Jeong, M. *Macromolecules* **2002**, *35*, 9794−9798.
(26) Dijkstra, M.; Frenkel, D.; Hansen, J.-P. *J. Chem. Phys.* **1994**, *101*, 3179−3189.
(27) Note that the restrictions on r_x, r_y, r_z and the taking of absolute value signs around r_x, r_y, r_z were not explicitly stated in ref 25, but they have to be present for eq 20 to be well-defined.
(28) Read, D. J. *Macromolecules* **1998**, *31*, 899−911.

MA0203851